Title: Hollow-fiber membrane technology: Characterization and proposed use as a potential mimic of skin vascularization towards the development of a novel skin absorption *in vitro* model

Authors: Patricia Perez Esteban, Juliette Pickles, Andrew D. Scott, Marianne J. Ellis

PII: S1369-703X(19)30039-7
DOI: https://doi.org/10.1016/j.bej.2019.01.025
Reference: BEJ 7147

To appear in: *Biochemical Engineering Journal*

Received date: 23 July 2018
Revised date: 18 December 2018
Accepted date: 30 January 2019

Please cite this article as: Perez Esteban P, Pickles J, Scott AD, Ellis MJ, Hollow-fiber membrane technology: Characterization and proposed use as a potential mimic of skin vascularization towards the development of a novel skin absorption *in vitro* model, *Biochemical Engineering Journal* (2019), https://doi.org/10.1016/j.bej.2019.01.025

Hollow-fiber membrane technology: Characterization and proposed use as a potential mimic of skin vascularization towards the development of a novel skin absorption *in vitro* model

Patricia Perez Esteban [a b], Juliette Pickles [c], Andrew D. Scott [c], Marianne J. Ellis [a*]

[a]*Department of Chemical Engineering and Centre for Regenerative Medicine, University of Bath, Claverton Down BA2 7AY, Bath, UK*

[b]*School of Life & Health Sciences, Aston University, Aston Triangle, Birmingham, B4 7ET, UK*

[c]*Safety and Environmental Assurance Centre, Unilever, Colworth Park, Sharnbrook, Bedfordshire, MK44 1LQ UK*

*Author to whom correspondence should be addressed: Marianne J. Ellis

Highlights:

- Hollow fiber membranes have been manufactured using a novel material, achieving a porous surface via the addition of a porogen agent.
- The surface of hollow fiber membranes has been functionalized so their polarity can be tailored according to their desired application.
- The permeation of caffeine through the fibrous structure has been measured for both hydrophobic and hydrophilic fibers.
- Both the rate of permeation and the degree of blocking for hydrophilic fibers is much higher than those for hydrophobic fibers, suggesting the presence of interactions between caffeine molecules and surface functional groups.
- The existence of spontaneous permeation constitutes an excellent starting point for the use of *polystyrene* hollow fibers as 'pseudo-capillaries' in skin vascularization.

Abstract

Dermal bioavailability is currently estimated through skin penetration studies using *ex vivo* models, which lack any measure of capillary bed function, and thus do not fully reproduce physiological conditions. We propose a novel strategy to mimic skin vascularization using newly fabricated hollow fibers made from a biocompatible membrane material, *polystyrene*, which is hydrophobic if left untreated, or hydrophilic when its surface polarity is modified through plasma-treatment. Caffeine has been well studied in skin penetration assays and was used here to determine the permeation properties of the hollow fibers in a novel jacketed glass bioreactor. For hydrophobic fibers, approximately 87.2 % of the caffeine dose did not penetrate the porous surface; 0.2 % of the dose was collected after 24 h (permeated through the pores), and therefore 12.6 % of the initial dose was suspected to block the membrane. For hydrophilic fibers, both the percentage of the initial dose that permeated and that of blocking caffeine increased to 1.2 % and 35.2 % respectively. It was concluded that caffeine permeated the hollow fibers at similar times of clearance to those observed *in vivo*, and therefore shows that this new model could provide a surrogate for capillary-based clearance in *in vitro* skin absorption studies.

Keywords: Skin penetration; tissue engineering; systemic toxicity; hollow fiber membranes; chemical adsorption.

1. Introduction

The study of the absorption of different chemicals, from topical drug and cosmetic formulations into and through the skin is key for the assessment of their safety. This is important for pharmaceutical and cosmetic companies to determine how much of a compound enters the blood stream and therefore the rest of the body – the systemic dose. Delivery of certain compounds via the topical route reaching the systemic circulation is of particular importance, since drug delivery to the skin is well accepted by patients [1], as opposed to other administration methods. Additionally, consumers may be exposed to many products via the dermal route, from cosmetics and household products to pesticides. Internationally accepted guidance for skin penetration studies has been produced by organizations such as the Organization for

Economic Cooperation and Development (OECD, guidelines 428 and 28) [2, 3], and the Scientific Committee on Consumer Safety [4]. Data generated using these methods are relied upon for safety decision making, both in various fields of industry and by regulators such as the Food and Drug Administration (FDA) in the United States [5]. Given the complexity and multi-functional properties of skin [6, 7], obtaining an accurate representation of the skin absorption process is complex, where the ideal would be analysis of absorption through the skin *in vivo*, and preferably human *in vivo*. However, there are practical and ethical issues leading to a drive in the reduction of *in vivo* animal testing [8], while *in vivo* human clinical studies may be expensive, highly regulated and require the generation of large amounts of safety data in advance of a study. Extrapolation from inter-species *in vivo* data may also prove challenging; when performing an *in vitro* assay, access to *ex vivo* human skin allows testing to be performed in the species of interest.

Considering *in vitro* assays, there are technical difficulties when comparing results obtained using different methods, species, or ages [7]. There exist a number of *in vitro* models that aim to mimic percutaneous absorption *in vivo*. They are classified according to Howes et al. as a function of their similarities with respect to the *in vivo* situation [9]. It is worth highlighting the so-called 'Perfused Skin Models', which are regarded as the most appropriate compromise between *in vivo* and *in vitro* methods but are not widely used since they require surgical techniques on living animals to form the skin flap. Their main advantage is the presence of fully active skin microcirculation and metabolism [10-12], since a key aspect that hampers the concordance between *in vivo* and *in vitro* data is the fact that most compounds are cleared via the capillary vasculature that is located near the junction between the epidermis and dermis [13]. Vascularization of the skin has an important role in percutaneous absorption, and the presence of a higher number of blood vessels in certain parts of the body (such as the face) allows for the rapid clearance of applied substances [14]. The presence of follicles or skin appendages, in general, is also significant: as an example, Illel et al. [15] demonstrated that in the absence of hair follicles, the steady-state flux and the amounts diffusing in 24 or 48 h were up to four times lower than in normal skin in rats. Hair follicles function as preferential pathways for diffusion for certain molecules. However, most routine skin penetration assays use dermatomed skin, which lacks any form of functional vascularization, but still retains the appendages, which may act as a better route than *in vivo*, where sebum

flow may reduce efficiency of absorption. Dermatomed skin is used to compensate for the lack of active circulation, reducing the depth of the dermis through which penetrating compounds must pass to reach the receptor solution. The dermis is a water-rich compartment, and may present a significant barrier to penetration for lipophilic materials [6].

One of the strategies that has been traditionally used to identify the limitations of the *in vitro* methods consists of the theoretical analysis and development of correlations that relate the physicochemical properties of the permeants to the mechanistic aspects of skin permeability [16, 17]. Some of the features that are studied and compared are the amount excreted as a percentage of the applied topical dose [18], the flux, cumulative flux, cumulative mass, and permeability [19]. The concordance between *in vivo* and *in vitro* data dramatically depends on the nature of the compounds that permeate and the liquid vehicle in which they are dissolved and dosed [20], together with the type and/or thickness of the skin that is used in the experimental method. It has been shown that there is a reasonably good prediction for a number of chemicals, but the difference between *in vitro* and *in vivo* results is greater for lipophilic molecules that are retained in the stratum corneum (lipid-rich) in the absence of circulation [21].

In view of the current limitations of skin penetration techniques, the introduction of some form of pseudo-vascularization may offer an increase in the *in vivo* relevance of the current widely accepted *in vitro* technique. From a tissue engineering perspective, the challenge of introducing pseudo-vascularization in skin models can be tackled in broadly two ways. Tissue engineering as a discipline involves the application of engineering and life sciences principles to create biological tissue substitutes, in the form of full organs for instance, to restore, maintain or improve tissue function [22]. One of the most common strategies used in tissue engineering is the construction of scaffolds that allow cultivation of tissue cells in a three-dimensional environment, where they have access to efficient nutrition and release of waste products. Some examples of the application of tissue engineering can be found in the area of bone regeneration [23, 24], culture of liver cells [25, 26], and particularly relevant for skin vascularization and angiogenesis, some biomaterials have been developed to induce growth of new blood vessels [27]. Our approach faces the same challenge as that presented in the work by Gigliobianco et al. [27], e.g. the limitations due to the lack of vascularization in *in vitro* models, but aiming to include completely artificial blood

vessels, formed by hollow fibers. Hollow fibers have been shown to be an excellent tool in tissue engineering applications [28-30], and the basis of this work consists of the inclusion of such hollow fibers as 'pseudo-capillaries' in *in vitro* skin absorption models. Here we aim to investigate, as a proof of concept, the characterization of polymeric hollow fiber membranes in terms of caffeine permeability, and the influence of their surface polarity on the caffeine flux that enters the pores located on their outer surface and is carried through their lumen mimicking the blood flow. Caffeine was used as a standard compound in percutaneous permeation, as indicated by the OECD guidelines 428 and 28 [2, 3]. This will establish the basic technology that can potentially be added to the current *in vitro* skin permeation models for an improved representation of *in vivo* clearance.

2. Materials and methods

2.1. Materials

Caffeine powder (ReagentPlus®), sodium chloride, and polystyrene (as nurdles, average MW ~280,000) were purchased from Sigma-Aldrich (Dorset, UK). 1-Methyl-2-pyrollidone was purchased from Acros Organics (Fisher Scientific, Loughborough, UK).

2.2. Hollow fiber fabrication

Casting dopes were formulated using 10 g of polystyrene, and 4 g of NaCl crystals of defined and controlled size, as described by Argyle at al. [31]. Initially, the salt crystals were dispersed in 19.45 ml of n-methyl-2-pyrollidone (NMP) overnight, and the polymer was then added to the salt-solvent mixture, and incubated at 37 °C, continuously mixed for 24 hours until fully incorporated. The relative salt mass to polymer mass is 40 %; hence the hollow fibers in this work are referred to as *PX40* fibers for simplicity. Hollow fibers were prepared by the wet spinning technique as described elsewhere [28]. The tank containing the polymer was well mixed prior to spinning in order to ensure uniform salt dispersion. Reverse osmosis (RO) water was used as the coagulant. Once the spinning process was terminated, the hollow fibers were immersed in RO water, which was changed every 12 hours for 3 days in order to completely remove both the solvent and salt creating a porous structure.

2.3. Hollow fiber characterization

Morphological characterization and qualitative analysis of the porosity of *PX40* fibers were performed using scanning electron microscopy (SEM). The fibers were immersed in liquid nitrogen and cut into small pieces of approximately 5 mm in length, prior to freeze-drying overnight. They were then sputter-coated with gold (Edwards Sputter Coater 5150B) and analyzed by SEM (JEOL JSM-6480LV) with an acceleration voltage of 10 kV. SEM micrographs of the inner and outer surfaces and the cross-sections of the hollow fibers were obtained.

2.4. Hollow fiber surface modification

PX40 fibers are intrinsically hydrophobic as demonstrated by Argyle et al. [31] via measurements of contact angle. However, their surface polarity can be modified. After the fibers were dried, they were subjected to low pressure oxygen plasma treatment for five minutes (25 W) using a ZEPTO Plasma cleaner (Deiner Electronic) in order to modify the functional groups that are present on the polymer surface, increasing its hydrophilicity.

2.5. Caffeine permeation studies

To determine the permeation of caffeine from the outer porous surface of *PX40* hollow fibers to their lumen – mimicking the process that occurs in capillary blood vessels – a custom-made glass bioreactor was designed, which allows for temperature control (Figure 1).

It consisted of an inner glass tube where the hollow fiber was placed, and an outer jacket that was connected to a water bath in order to maintain a constant temperature. Since in the standard skin permeation experiments currently used in industry the skin surface is at 32 °C, as is the receptor fluid, the temperature of the water bath was set at 32 °C, and water was constantly recirculated at a flow rate of approximately 1.2 liters min^{-1}. Heat losses in the tubing and through the glass walls were considered negligible. A single dose of 0.5 ml caffeine solution (7.5 mg ml^{-1}) was incorporated in the inner glass tube, i.e. completely filling the extra-capillary space around the *PX40* fiber. A constant flow of deionized water was circulated through the lumen of the fiber at a flow rate of 2.5 ml h^{-1} (which corresponds to a mean velocity of 3.4 cm min^{-1}, or 0.6 mm s^{-1}, given that the diameter of the hollow fiber is approximately 1 mm). This flow rate was selected in order to reproduce the conditions that are normally

used in the conventional flow cells in skin penetration assays [32, 33], and it is within the range that has historically been measured for capillary blood cell velocities [34, 35]. A flow rate of 2.5 ml h^{-1} is considered high enough to create sink conditions and thus diffusion is unconstrained by the creation of high local concentrations [7].

The design of the custom-made glass bioreactor allows for multiple fibers (up to three in parallel). In this particular case, it contained a single hollow fiber of 10 cm in length, with an extra 2 cm on each side as shown in Figure 1. The additional length of both sides was not subject to permeation, as it was not in contact with the dose solution. The choice of a single hollow fiber was based on the equivalent surface area covered by the blood capillary loops that sit between the dermis and epidermis in a skin disk of approximately 0.45 cm radius (surface area 63.6 mm^2), which is the standard disk size in skin penetration cells [36]. The geometrical properties of the capillaries were extracted from the work by Kretsos et al. [37] and summarized in Table 1.

The length of loop was considered for calculations, since it is the part of the capillary that is potentially in direct contact with the substance that penetrates the skin in the first place. The number of capillaries and the total surface area (SA) that would hypothetically exist in the skin disk is shown in Equations 1 and 2 respectively.

$$n_{capillaries} = \frac{10^8 capillaries}{m^2} \times 6.36 \times 10^{-5} m^2 = 6.36 \times 10^3 \; capillaries \quad \textbf{Equation 1}$$

$$SA_{capillaries} = n_{capillaries}\, 2\, \pi\, r_{capillaries}\; L_{capillary} = 3.0 \times 10^{-5} m^2 \quad \textbf{Equation 2}$$

Where $n_{capillaries}$ is the number of blood capillaries (-) in the 0.45 cm-radius skin disk, $SA_{capillaries}$ is the total surface area available for absorption (m^2), $r_{capillary}$ is the radius of the capillary loop (m), and $L_{capillary}$ is the length of the capillary loop (m).

The total surface area shown in Equation 2 was matched with the surface area available for permeation in the hollow fibers, taking into account the properties of *PX40* fibers (shown in Table 2).

The length of the hollow fiber was therefore calculated according to Equation 3.

$$L_{fiber} = \frac{SA_{capillaries}}{2\,\pi\, r_{fiber}\, \gamma_{fiber}} \approx 10\ cm \qquad \textbf{Equation 3}$$

Where L_{fibre} is the length of the hollow fiber (m), $SA_{capillaries}$ is the total surface area available for absorption (m^2), r_{fiber} is the radius of the hollow fiber (m) and γ_{fiber} is the porosity of the hollow fiber (-).

Samples from the lumen outlet were taken every ten minutes for two hours, and in a second experiment every hour for 24 hours, and the concentration of caffeine was analyzed via HPLC (Agilent Technologies, 1260 Infinity Series). The concentration of caffeine was calculated directly comparing the area of the peaks measured via HPLC with the calibration curve obtained with caffeine standards of known concentration. The integration of the peaks was performed manually. A C18 column was used (Poroshell 120 EC-C18, 2.7 μm, 4.6 x 50 mm), and isocratic elution was chosen. The mobile phase was 75:25 acetonitrile: deionized water, and a UV-visible detector was employed (DAD Detector Signal (mAU) = 273/4 nm, Reference 360/80 nm). A calibration using caffeine solutions of known concentration was performed. The retention time of caffeine in the column used for this study was approximately 0.54 minutes.

Where appropriate, cumulative masses were determined as the sum of the mass of permeated caffeine at a certain time point plus the mass at all previous time points; and fluxes were calculated as the mass of permeated caffeine divided by the time and the surface area of the 10 cm hollow fiber.

2.6. Statistical analysis and data accessibility

All the results are presented as the average value from three (N = 3) independent experiments and the error bars represent the standard deviation. One-tailed Student's *t-test* at a 95 % confidence level was used to assess significant differences between independent samples where appropriate.

3. Results and Discussion

3.1. Morphology and porosity of hollow fibers

The hollow fiber's surface at a magnification of X5,000 can be seen in Figure 2A, and the results shown here are consistent with the work by Argyle et al. [31]; pores of approximately 1 μm in diameter can be observed. The presence of a higher concentration of porogen would increase the number of pores per unit surface area [31]. Figure 2B (magnification of X60) shows the cross section of the *PX40* hollow fiber. Its asymmetric structure shows the clear narrowing of pores from top to bottom. The outer surface is smooth with randomly distributed pores (as seen in Figure 2A), whereas the sub-structure consists of uniform macrovoids. It can also be seen that the cross section is not regular with respect to the thickness of the walls. This is due to variations in the wet spinning manufacture (particularly because of the position of the needle through which water is circulated in order to create the hollow lumen of the fiber).

3.2. Caffeine permeation in hydrophobic and hydrophilic fibers for 2 hours

The concentration of caffeine (7.5 mg ml^{-1}) can be considered as an infinite dose, i.e., the time for all the caffeine in the dose to permeate through the porous hollow fiber is long enough to be regarded as infinite assuming that no blocking of the pores occurs. Infinite dose scenarios are commonly used in skin penetration assays, since they allow a maximum rate of absorption to be maintained over time, and it is therefore possible to calculate steady state parameters [38]. This study was initially conducted for 2 hours to observe the initial moments of permeation before reaching steady state. The concentration profile of caffeine permeating through the porous outer surface of *PX40* hydrophobic hollow fibers is shown in Figure 3A, and that for hydrophilic hollow fibers can be seen in Figure 3B. Caffeine is carried through the lumen of the fibers by the external flow of deionized water via convection, simulating blood circulation.

It is clear that the permeation rate over a period of two hours dramatically depends on the polarity of the surface of the membrane. In the case of hydrophobic fibers (Figure 3A) the concentration of caffeine in the permeate remains roughly constant for 30 minutes, and then increases until it reaches a plateau by the end of the experiment. For hydrophilic fibers (Figure 3B), the concentration of caffeine that permeates is initially (at 10 minutes) 200 times higher than that for hydrophobic fibers (~10 μg ml^{-1} versus ~0.05 μg ml^{-1}). The concentration is constant for approximately 20 minutes and then increases, reaching its maximum at circa 50 minutes. It is worth highlighting that the maximum concentration achieved using hydrophilic fibers is ~285 times higher than

the corresponding maximum concentration for hydrophobic fibers (~50 μg ml^{-1} versus ~0.18 μg ml^{-1}). The concentration of caffeine, in the permeate, in hydrophilic *PX40* decreases slowly after 60 minutes, and the trend observed in Figure 3B suggests that a plateau would be reached. These results are consistent with the relatively hydrophilic nature of caffeine (partition coefficient water/n-octanol logP = -0.55).

The experimental data in Figures 3 A and B can be used to obtain the steady state values of caffeine concentration (despite not being reached after 2 hours). It can be seen that the shapes of the curves are broadly comparable: they both consist of an initial lag phase, followed by an increase in concentration, and then a decrease; despite the differences in permeation times and rates, suggesting that the mechanisms of permeation are analogous regardless of the polarity of the fibers. A third order polynomial fitting was applied to the first part of both curves seen in Figures 3 A and 3 B as the curve of best fit, when the concentration of caffeine increases, as follows:

$$C_{caffeine} = a_0 + a_1\, t + a_2\, t^2 + a_3\, t^3 \qquad \textbf{Equation 4}$$

Following this, the peaks of both curves and the consequent decay in concentration were modeled using a quadratic fitting, as the curve of best fit, according to Equation 5:

$$C_{caffeine} = b_0 + b_1\, t + b_2\, t^2 \qquad \textbf{Equation 5}$$

Where $C_{caffeine}$ is the concentration of caffeine (μg ml^{-1}), a_0 (μg ml^{-1}), a_1 (μg ml^{-1} h^{-1}), a_2 (μg ml^{-1} h^{-2}), a_3 (μg ml^{-1} h^{-3}), b_0 (μg ml^{-1}), b_1 (μg ml^{-1} h^{-1}), and b_2 (μg ml^{-1} h^{-2}) are parameters for the fittings, and t is the time (h).

Predicted values can be calculated fitting the data to the corresponding equations, using non-linear least square minimization. The resulting parameters for the fittings shown in Figures 3 A and 3 B can be seen in Table 3. It also includes the prediction of the steady state concentration of caffeine after a virtually infinite time (7 days) in order to test the validity of the experimental model proposed in Equations 4 and 5.

The predicted values shown in Table 3 were then confirmed experimentally. It was found that the experimental model slightly over-predicts the concentration of caffeine after 7 days. This may be due to the blocking of the pores with time.

Differences when comparing the flux of caffeine through hydrophobic (Figure 4A) and hydrophilic (Figure 4B) fibers, and in the cumulative mass that is collected after 2 hours (Figure 5) can be observed. Fluxes were calculated taking into account the surface area of the hollow fiber, which has an average diameter of ~1 mm and a length of 10 cm. The fluxes in Figure 4 show practically identical trends as the ones seen in Figure 3 for the concentration of caffeine. The maximum flux achieved in hydrophobic *PX40* was 0.15 μg cm^{-2} h^{-1}, while the maximum flux for hydrophilic *PX40* was 65 μg cm^{-2} h^{-1}. In addition to this, Figure 4 shows the differences in flux when hollow fibers were used in a first and a second pass (after being cleaned and flushed). For hydrophobic fibers (Figure 4A) there are no significant differences between the flux in the first and second passes; in fact, they overlap at approximately 50 minutes, although the flux is marginally smaller by the end of the experimental time in the second pass. On the other hand, significant differences can be seen between the flux in the first and second passes for hydrophilic fibers. The evolution of flux over time is similar for both first and second passes (relatively flat start followed by an increase and then a smooth decrease), as can be seen in Figure 4B, but the magnitude of the flux is noticeably different – the maximum flux in the first pass is almost 6 times higher than in the second pass. This fact suggests that hydrophilic fibers undergo irreversible blocking of the pores.

The same conclusion can be reached by observing the cumulative mass of caffeine that permeates in a first and second passes, as shown in Figure 5. The final cumulative mass after 2 hours in the first and second passes for hydrophobic fibers is statistically the same, whereas for hydrophilic fibers, the final cumulative mass is significantly higher in the first pass than in the second pass (P-value = 0.0003, see Figures 5C and 5D).

Concerning the possible fouling or blocking phenomena occurring in the porous structure of *PX40* hollow fibers, membranes with hydrophilic surfaces are less susceptible to fouling [39]. This obviously depends on the polarity of the foulants. An increase in the hydrophilicity of the membrane surface is often used to reduce membrane fouling by organic pollutants and microorganisms. Due to the formation of

hydrogen bonds, a thin layer of bounded water exists on the surface of the hydrophilic membrane. This layer can prevent or reduce undesirable adsorption or adhesion of the compounds on the membrane surface [39]. In the case of caffeine, we hypothesize that these hydrogen bonds due to the functional groups of the membrane surface can also be formed with the caffeine molecules, inducing blocking.

3.3. Caffeine permeation rates

In order to determine the rate of permeation of caffeine through hydrophilic and hydrophobic *PX40* hollow fibers, the permeation study was extended over 24 hours and the relative cumulative mass at every time point with respect to the cumulative mass at the initial time (1 hour) was calculated. A period of 24 hours was considered in this case since it constitutes the standard time for skin penetration assays [6]. These results are shown in Figure 6, together with a linear fitting in order to calculate the permeation rates, according to Equation 6 as follows:

$$\frac{Cumulative\ Mass\ (t)}{Cumulative\ Mass\ (t_0)} = a + k\ t \qquad \textbf{Equation 6}$$

Where a is a constant (dimensionless), k is the permeation rate (h^{-1}) and t is the time (h). The parameter a is 0, since there is no permeation of caffeine at time 0.

The permeation rate of caffeine in hydrophobic fibers was found to be 0.61±0.03 h^{-1}, while the permeation rate in hydrophilic fibers was 1.63±0.01 h^{-1}. This difference in caffeine permeation kinetics in hydrophobic and hydrophilic environments has been observed in the literature, when comparing caffeine permeation in skin that presented hair follicles (which is considered as the preferential pathway for hydrophilic compounds, although there is some controversy in the literature surrounding this fact) and with no appendages at all [40, 41].

As far as the percentage of dose that permeates is concerned, in terms of cumulative mass in the permeate, for hydrophobic fibers, approximately 87.2 % of the caffeine dose did not penetrate the porous surface of the fiber; 0.2 % of the dose was collected after 24 h (permeated through the pores), and therefore 12.6 % of the initial dose was suspected to block the membrane. For hydrophilic fibers, both the percentage of the initial dose that permeated and that of blocking caffeine increased to 1.2 % and 35.2 % respectively.

The results in this work can be compared to *in vivo* caffeine skin penetration data. The *in vivo* results obtained by Otberg *et al*. [40, 41] showed penetration of caffeine into the blood is rapid, following topical application, detectable in the blood after only a few minutes and reaching its maximum after 1 hour, and is similar to the results shown here for hydrophilic fibers (Figure 3 B). Otberg *et al*. [40, 41] also demonstrated that caffeine penetration is faster *in vivo* rather than *in vitro*, probably due to the existent blood flow *in vivo*. Those conditions are appropriately mimicked by the hollow fibers in this study. On the other hand, the percentage of caffeine that permeates after 24 hours is lower than that reported *in vivo* (between 12.4 and 24.9 %), mainly because of the blocking of the pores in the hollow fibers.

Conclusions

We have fabricated hollow fiber membranes using a novel material, '*polystyrene*', and functionalized the surface properties of the fibers such that their polarity can be tailored according to their use. Caffeine is a widely studied chemical in skin penetration assays and as a proof of concept study we have demonstrated that caffeine permeates hydrophilic polystyrene hollow fibers. Having established that caffeine can penetrate the fibers, they will be appropriate in order to mimic permeation into and movement through skin capillaries. The presence of an artificial vasculature will help overcome some of the limitations of the current established models, namely the inclusion of fully functioning 'vascular network', which is essential for the clearance of absorbed compounds that occurs in an *in vivo* scenario. Their use as a surrogate for capillary-based clearance in *in vitro* skin absorption studies will be the focus for further work.

Data access statement

All data created during this research is openly available from the University of Bath Research Data Archive at https://doi.org/10.15125/BATH-00579 [42]

Acknowledgements

The authors wish to acknowledge financial support from the National Centre for the Replacement, Refinement & Reduction of Animals in Research (NC3Rs), Innovate UK and the Engineering and Physical Sciences Research Council (EPSRC). We also

thank Dr. Alexander Ciupa, Mr. David Sanders and Ms. Ruth Pendlington for technical assistance.

References

[1] S. Wiedersberg, R.H. Guy, Transdermal drug delivery: 30+ years of war and still fighting!, J. Control Release 190 (2014) 150-6.

[2] OECD, Skin Absorption: In Vitro Method, in: OECD (Ed.) Test guideline 428, Paris, 2004.

[3] OECD, Guidance document for the conduct of skin adsorption studies, in: OECD (Ed.) Series on Testing and Assessment. No 28, Environment Directorate, Paris, 2004.

[4] SCCNFP, Basic criteria for the in-vitro assessment of dermal absorption of cosmetic ingrecients, in: SCCNFP (Ed.) Burssels, 2010.

[5] FDA, Guidance for industry: SUPAC-SS In-vitro release testing and in-vivo bioequivalence documentation, in: CDER (Ed.) 1997.

[6] D.A. Bucks, Skin structure and metabolism: Relevance to the design of cutaneous therapeutics, Pharm Res 1(4) (1984) 148-53.

[7] U.F. Schaefer, S. Hansen, M. Schneider, J.L. Contreras, C.-M. Lehr, Models for Skin Absorption and Skin Toxicity Testing, in: C. Ehrhardt, K.-J. Kim (Eds.), Drug Absorption Studies: In Situ, In Vitro and In Silico Models (2007) 3-33.

[8] R.P. Chilcott, Cutaneous anatomy and function, Principles and practice of skin toxicology (2008) 1-16.

[9] D. Howes, R. Guy, J. Hadgraft, J. Heylings, U. Hoeck, F. Kemper, H. Maibach, J.-P. Marty, H. Merk, J. Parra, D. Rekkas, I. Rondelli, H. Schaefer, U. Taeuber, N. Verbiese, Methods for Assessing Percutaneous Absorption. The Report and Recommendations of ECVAM Workshop 13, Altern. Lab. Anim. 24 (1996) 81-106.

[10] J.E. Riviere, K.F. Bowman, N.A. Monteiro-Riviere, On the definition of viability in isolated perfused skin preparations, Br. J. Dematol. 116 (1987) 739-741.

[11] J.E. Riviere, K.F. Bowman, N.A. Monteiro-Riviere, L.P. Dix, M.P. Carver, The isolated perfused porcine skin flap (IPPSF). I. A novel in vitro model for percutaneous absorption and cutaneous toxicology studies, Fundam. Appl. Toxicol. 7(3) (1986) 444-453.

[12] J.E. Riviere, N.A. Monteiro-Riviere, The Isolated Perfused Porcine Skin Flap as an *In Vitro* Model for Percutaneous Absorption and Cutaneous Toxicology, Critical Reviews in Toxicology 21(5) (1991) 329-344.

[13] D.R. Friend, In vitro skin permeation techniques, Journal of Controlled Release 18 (1992) 235-248.

[14] H. Tagami, Percutaneous Absorption and Principles of Corneotherapy/Skin Care, in: T. Krieg, D.R. Bickers, Y. Miyachi (Eds.), Therapy of Skin Diseases: A Worldwide Perspective on Therapeutic Approaches and Their Molecular Basis, Springer Science & Business Media (2010) 57-61.

[15] B. Illel, H. Schaefer, J. Wepierre, O. Doucet, Follicles play an important role in percutaneous absorption, Journal of Pharmaceutical Sciences 80(5) (1991) 424-427.

[16] R.O. Potts, R. Guy, Predicting Skin Permeability, Pharmaceutical Research 9(5) (1992) 663-669.

[17] A. Wilschut, W.F. ten Berge, P.J. Robinson, T.E. McKone, Estimating skin permeation. The validation of five mathematical skin permeation models, Chemosphere 30(7) (1995) 1275-96.

[18] R.L. Bronaugh, R.F. Stewart, E.R. Congdon, A.L. Giles, Jr., Methods for *in Vitro* percutaneous absorption studies. I. Comparison with *in Vivo* results, Toxicol Appl Pharmacol 62(3) (1982) 474-480.

[19] Q. Yang, R.H. Guy, Characterisation of skin barrier function using bioengineering and biophysical techniques, Pharmaceutical Research 32(2) (2014) 445-457.

[20] L. Chen, L. Han, G. Lian, Recent advances in predicting skin permeability of hydrophilic solutes, Adv Drug Deliv Rev 65(2) (2013) 295-305.

[21] F.M. Williams, In vitro studies—how good are they at replacing in vivo studies for measurement of skin absorption?, Environmental toxicology and pharmacology 21(2) (2006) 199-203.

[22] I. Martin, D. Wendt, M. Heberer, The role of bioreactors in tissue engineering, TRENDS in Biotechnology 22(2) (2004) 80-86.

[23] J.B. Chaudhuri, M.G. Davidson, M.J. Ellis, M.D. Jones, X. Wu, Fabrication of Honeycomb-Structured Poly(DL-lactide) and Poly[(DL-lactide)-co-glycolide)] Films and their Use as Scaffolds for Osteoblast-Like Cell Culture, Macromolecular Symposia 272(1) (2008) 52-57.

[24] S.M. Morgan, S. Tilley, S. Perera, M.J. Ellis, J. Kanczler, J.B. Chaudhuri, R.O. Oreffo, Expansion of human bone marrow stromal cells on poly-(DL-lactide-co-glycolide) (PDL LGA) hollow fibres designed for use in skeletal tissue engineering, Biomaterials 28(35) (2007) 5332-43.

[25] A.J. Davidson, M.J. Ellis, J.B. Chaudhuri, A theoretical method to improve and optimize the design of bioartificial livers, Biotechnol Bioeng 106(6) (2010) 980-8.

[26] A.J. Davidson, M.J. Ellis, J.B. Chaudhuri, A theoretical approach to zonation in a bioartificial liver, Biotechnol Bioeng 109(1) (2012) 234-43.

[27] G. Gigliobianco, C.K. Chong, S. MacNeil, Simple surface coating of electrospun poly-L-lactic acid scaffolds to induce angiogenesis, J Biomater Appl 30(1) (2015) 50-60.

[28] M.J. Ellis, J.B. Chaudhuri, Poly(lactic-co-glycolic acid) hollow fibre membranes for use as a tissue engineering scaffold, Biotechnol Bioeng 96(1) (2007) 177-87.

[29] H. Shearer, M.J. Ellis, S.P. Perera, J.B. Chaudhuri, Effects of common sterilization methods on the structure and properties of poly(D,L lactic-co-glycolic acid) scaffolds, Tissue Eng 12(10) (2006) 2717-27.

[30] N. Wung, S.M. Acott, D. Tosh, M.J. Ellis, Hollow fibre membrane bioreactors for tissue engineering applications, Biotechnol Lett 36(12) (2014) 2357-66.

[31] I.S. Argyle, M.P. Storm, M.J. Ellis, Common salt used as a pore forming agent in flat sheet and hollow fibre polymeric membrane synthesis (In Preparation), (n.d.).

[32] C.A. Moore, S.C. Wilkinson, P.G. Blain, M. Dunn, G.A. Aust, F.M. Williams, Percutaneous absorption and distribution of organophosphates (chlorpyrifos and dichlorvos) following dermal exposure and decontamination scenarios using in vitro human skin model, Toxicol Lett 229(1) (2014) 66-72.

[33] C.A. Moore, S.C. Wilkinson, P.G. Blain, M. Dunn, G.A. Aust, F.M. Williams, Use of a human skin in vitro model to investigate the influence of 'every-day' clothing and skin surface decontamination on the percutaneous penetration of organophosphates, Toxicol Lett 229(1) (2014) 257-64.

[34] K. Kellam, P. Altmeyer, Capillary blood cell velocity in human skin capillaries located perpendicularly to the skin surface: measured by a new laser Doppler anemometer, Microvascular research 52 (1996) 188-192.

[35] J. Ostergren, B. Fagrell, Skin capillary blood cell velocity in man. Characteristics and reproducibility of the reactive hyperemia response, International journal of microcirculation, clinical and experimental 5(1) (1986) 37-51.

[36] S.-F. Ng, J.J. Rouse, F.D. Sanderson, V. Meidan, G.M. Eccleston, Validation of a static Franz diffusion cell system for in vitro permeation studies, Aaps Pharmscitech 11(3) (2010) 1432-1441.

[37] K. Kretsos, G.B. Kasting, A geometrical model of dermal capillary clearance, Mathematical biosciences 208(2) (2007) 430-453.

[38] J. Kielhorn, S. Melching-Kollmuß, I. Mangelsdorf, Environmental Health Criteria 325 - Dermal Absorption, in: WHO (Ed.) WHO, 2006.

[39] V. Kochkodan, Reduction of Membrane Fouling by Polymer Surface Modification, in: N. Hilal, M. Khayet, C.J. Wright (Eds.), Membrane Modification: Technology and Applications, CRC Press Taylor & Francis Group, Boca Raton (2012) 41-76.

[40] N. Otberg, A. Patzelt, U. Rasulev, T. Hagemeister, M. Linscheid, R. Sinkgraven, W. Sterry, J. Lademann, The role of hair follicles in the percutaneous absorption of caffeine, Br J Clin Pharmacol 65(4) (2008) 488-92.

[41] S. Trauer, A. Patzelt, N. Otberg, F. Knorr, C. Rozycki, G. Balizs, R. Buttemeyer, M. Linscheid, M. Liebsch, J. Lademann, Permeation of topically applied caffeine through human skin--a comparison of in vivo and in vitro data, Br J Clin Pharmacol 68(2) (2009) 181-6.

[42] Ellis, M., 2019. Dataset for Hollow-fiber membrane technology: Characterization and proposed use as a potential mimic of skin vascularization towards the development of a novel skin absorption in vitro model. University of Bath Research Data Archive. https://doi.org/10.15125/BATH-00579

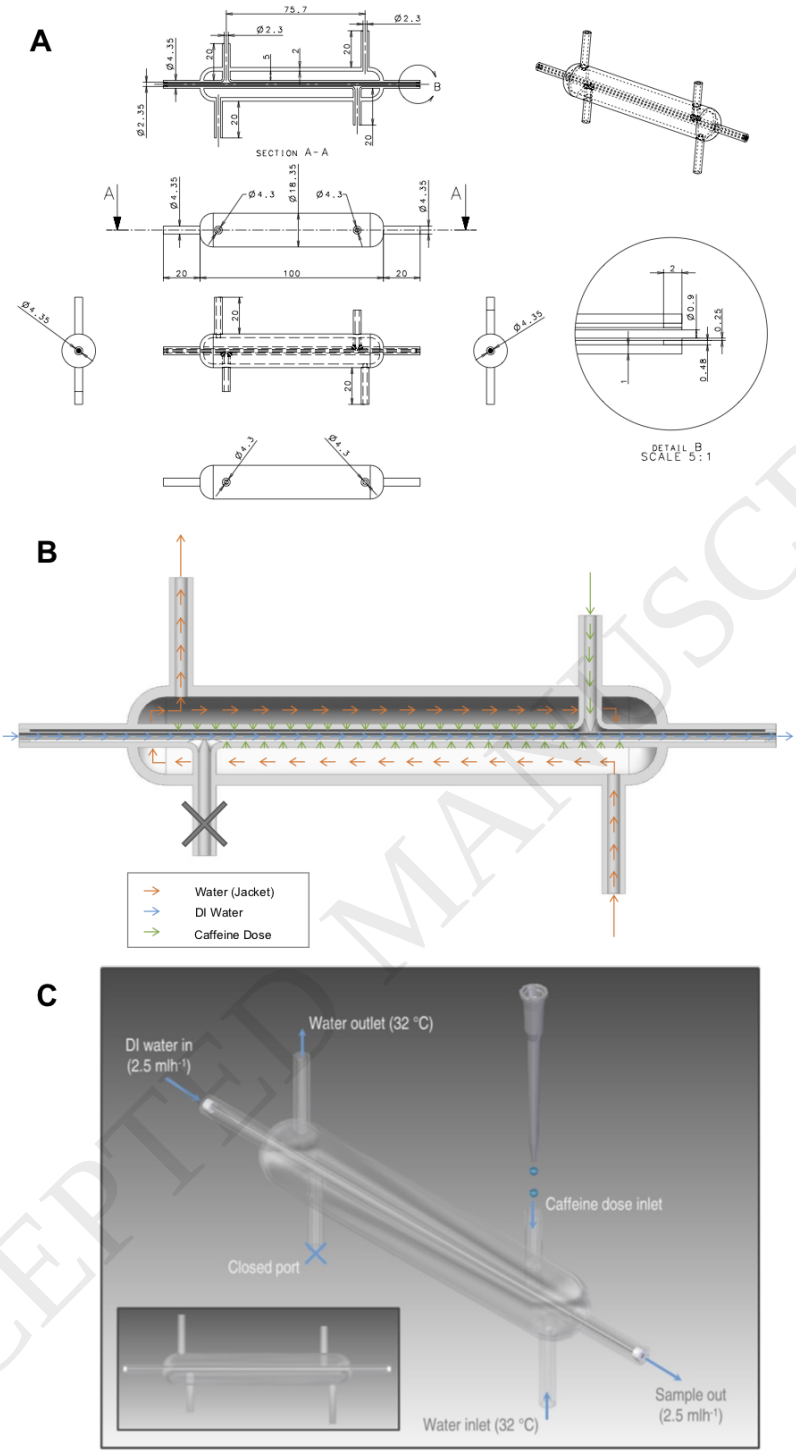

Figure 1: Caffeine permeation bioreactor system set-up.

(A) Technical drawing of the hollow fiber bioreactor, including all dimensions (in mm). (B) Two-dimensional view of the hollow fiber bioreactor. Arrows represent the flow of the different components. (C) Three-dimensional view of the hollow fiber bioreactor. The hollow fiber is placed within the inner glass tube. A single caffeine dose is introduced in the extra-capillary space. The outer glass tube constitutes the jacket through which

water at 32 °C is recirculated in order to maintain a constant temperature. Deionized (DI) water is pumped within the lumen of the fiber, carrying the caffeine that permeates across its porous surface. The inset represents a frontal view.

Figure 1: Caffeine permeation bioreactor system set-up.

(A) Technical drawing of the hollow fiber bioreactor, including all dimensions (in mm). (B) Two-dimensional view of the hollow fiber bioreactor. Arrows represent the flow of the different components. (C) Three-dimensional view of the hollow fiber bioreactor. The hollow fiber is placed within the inner glass tube. A single caffeine dose is introduced in the extra-capillary space. The outer glass tube constitutes the jacket through which water at 32 °C is recirculated in order to maintain a constant temperature. Deionized (DI) water is pumped within the lumen of the fiber, carrying the caffeine that permeates across its porous surface. The inset represents a frontal view.

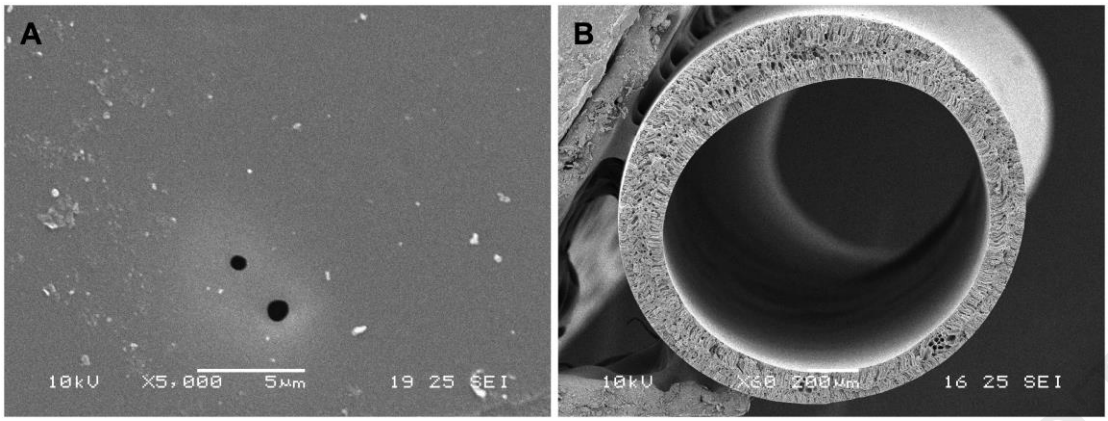

Figure 2: SEM of *PX40* hollow fiber. (A) Outer surface; (B) Cross section.

Pores of approximately 1 µm in diameter can be observed on the outer surface of the fiber. The porous structure of the fiber's wall is also evident in the image of its cross section.

Figure 2: SEM of *PX40* hollow fiber. (A) Outer surface; (B) Cross section.

Pores of approximately 1 µm in diameter can be observed on the outer surface of the fiber. The porous structure of the fiber's wall is also evident in the image of its cross section.

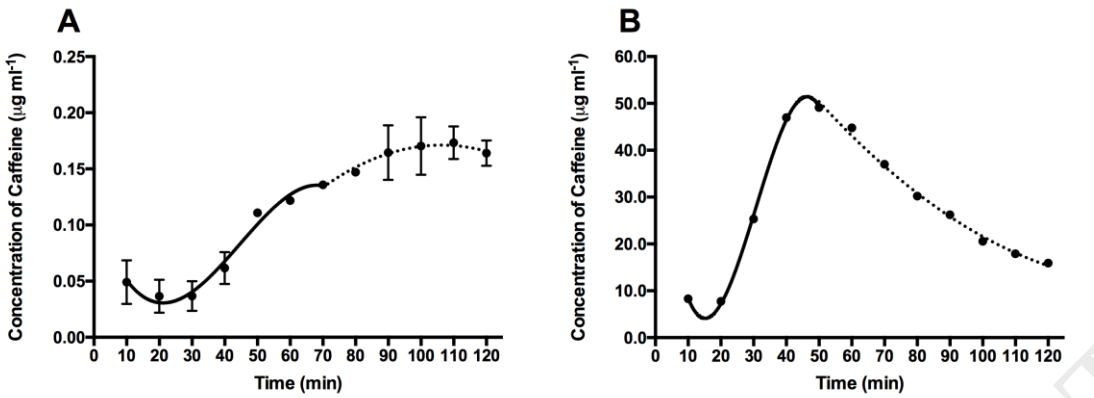

Figure 3: Comparison of the concentration of caffeine in permeates after 2 hours (A) Hydrophobic fibers; (B) Hydrophilic fibers. Fittings of the experimental data to determine the steady state values are also shown, namely a third degree polynomial and a quadratic fit for the first (solid line) and second (dotted line) part of the curves respectively.

(N = 3, Error bars represent the standard deviation of triplicates. Error bars that cannot be seen represent very small standard deviations).

Figure 3: Comparison of the concentration of caffeine in permeates after 2 hours (A) Hydrophobic fibers; (B) Hydrophilic fibers (N = 3, Error bars represent the standard deviation of triplicates).

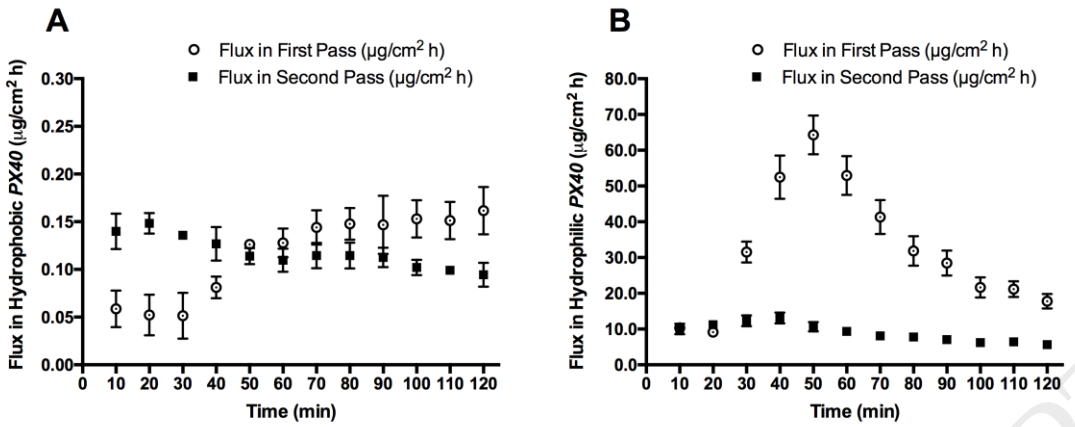

Figure 4: Flux of caffeine in hydrophobic fibers (A) and hydrophilic fibers (B) for fresh membranes (first pass), and used membranes (second pass).

(N = 3, Error bars represent the standard deviation of triplicates. Error bars that cannot be seen represent very small standard deviations).

Figure 4: Flux of caffeine in hydrophobic fibers (A) and hydrophilic fibers (B) for fresh membranes (first pass), and used membranes (second pass) (N = 3, Error bars represent the standard deviation of triplicates).

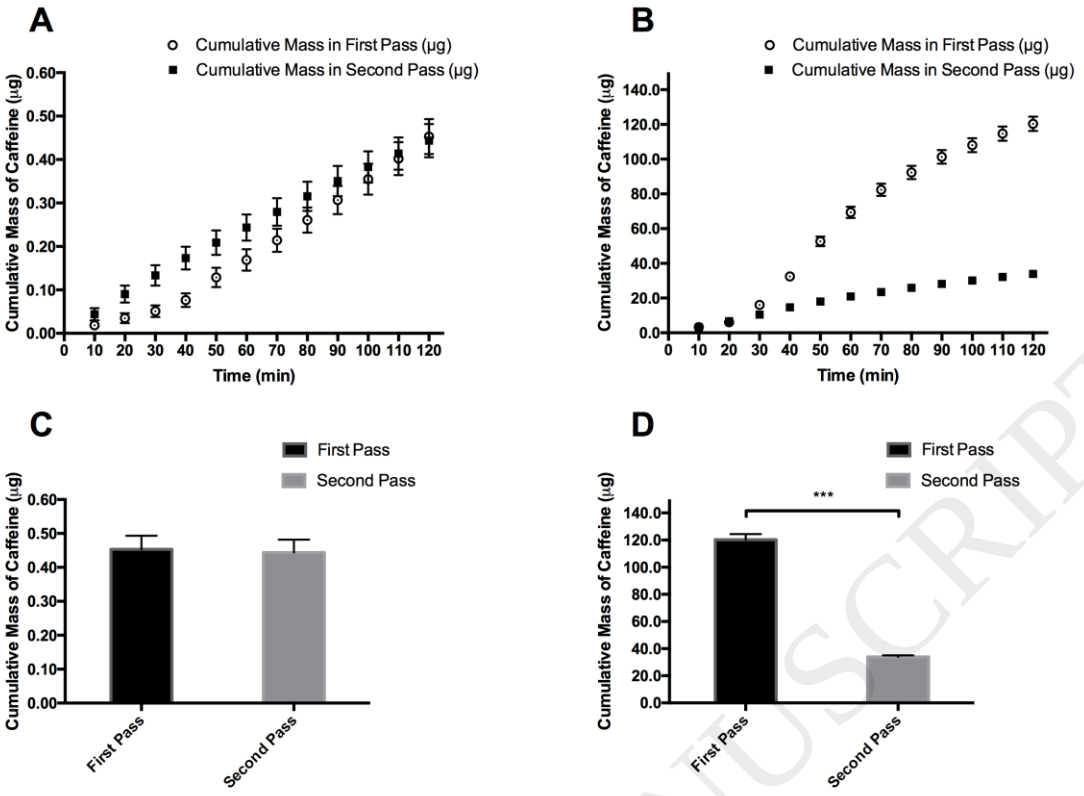

Figure 5: Cumulative mass of caffeine in hydrophobic fibers (A) and hydrophilic fibers (B) in both a first and second passes. The significance of pore blocking after a second pass is shown for hydrophobic fibers (C) and hydrophilic fibers (D).

(N = 3, Error bars represent the standard deviation of triplicates, *** p-value = 0.0003, 95 % Confidence).

Figure 5: Cumulative mass of caffeine in hydrophobic fibers (A) and hydrophilic fibers (B) in both a first and second pass. The significance of pore blocking after a second pass is shown for hydrophobic fibers in (C) and hydrophilic fibers in (D) (N = 3, Error bars represent the standard deviation of triplicates, *** p-value = 0.0003, 95 % Confidence).

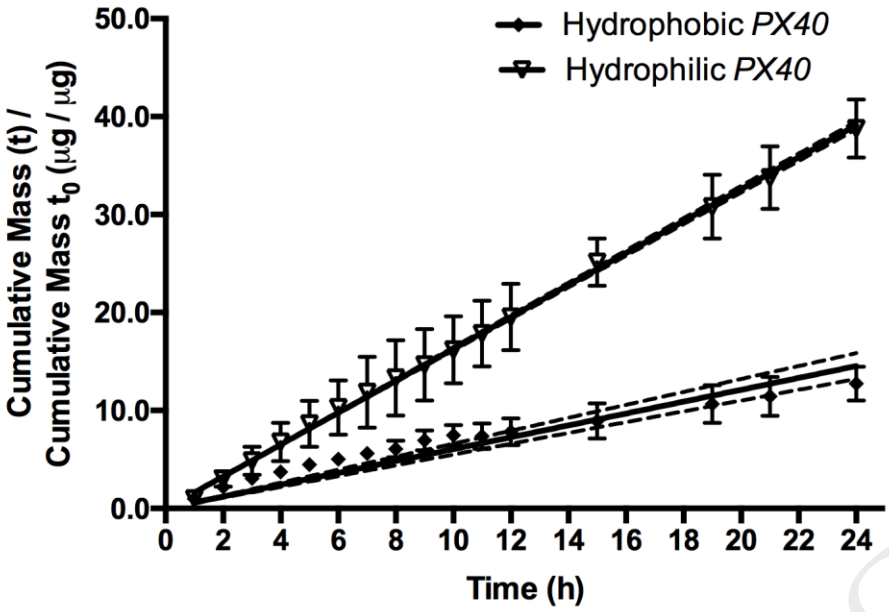

Figure 6: Permeation rate in both hydrophobic and hydrophilic fibers after 24 hours.

(N = 3, Error bars represent the standard deviation of triplicates). The discontinuous lines represent the 95 % confidence interval of the linear fittings.

Figure 6: Permeation rate in both hydrophobic and hydrophilic fibers after 24 hours (N = 3, Error bars represent the standard deviation of triplicates). The discontinuous lines represent the 95 % confidence interval of the linear fittings.

Table 1: Geometrical properties of dermal capillaries (adapted from [37]).

Property	Value
Length of loop	5×10^{-4} m
Radius	1.5×10^{-6} m
Capillary density	10^{8} capillaries per m^2

Table 2: Geometrical properties of *PX40* hollow fibers.

Property	Value
Porosity	0.1
Radius	485 x 10^{-6} m

Table 3: Fitting of experimental data for caffeine concentration for both hydrophobic and hydrophilic fibers.

Type of Fiber	Parameters	Prediction of caffeine concentration after 7 days	Measured caffeine concentration after 7 days
Hydrophobic (Figure 3 A)	$b_0 = -0.1522$ $b_1 = 0.006088$ $b_2 = -2.85 \times 10^{-5}$	0.07 μg ml^{-1}	(0.05 ± 0.02) μg ml^{-1} (N = 3)
Hydrophilic (Figure 3 B)	$b_0 = 97.99$ $b_1 = -1.141$ $b_2 = 0.003769$	12.7 μg ml^{-1}	(10.5 ± 0.8) μg ml^{-1} (N = 3)